International Journal of Solids and Structures 51 (2014) 430–439

Contents lists available at ScienceDirect

International Journal of Solids and Structures

journal homepage: www.elsevier.com/locate/ijsolstr

Finite inflation of a hyperelastic toroidal membrane over a cylindrical rim

Ganesh Tamadapu *, Anirvan DasGupta

Department of Mechanical Engineering, Indian Institute of Technology Kharagpur, Kharagpur 721302, India
Centre for Theoretical Studies, Indian Institute of Technology Kharagpur, Kharagpur 721302, India

ARTICLE INFO

Article history:
Received 5 July 2013
Received in revised form 2 October 2013
Available online 23 October 2013

Keywords:
Toroidal membrane
Large deformation
Contact mechanics
Cylindrical contact
Shooting method
Impending wrinkling

ABSTRACT

The present paper is devoted to the study of finite inflation of a hyperelastic toroidal membrane on a cylindrical rim under uniform internal pressure. Both compliant and rigid frictionless rims have been considered. The compliant cylindrical rim is modeled as a linear distributed stiffness. The initial cross-section of the torus is assumed to be circular, and the membrane material is assumed to be a homogeneous and isotropic Mooney–Rivlin solid. The problem is formulated as a two point boundary value problem and solved using a shooting method by employing the Nelder–Meads search technique. The optimization function is constructed on a two (three) dimensional search space for the compliant cylinder (rigid cylinder). The effect of the inflation pressure, material properties and elastic properties of the rim on the state of stretch and stress, and on the geometry of the inflated torus have been studied, and some interesting results have been obtained. The stability of the inflated configurations in terms of occurrence of the impending wrinkling state in the membrane has also been studied.

1. Introduction

Contact mechanics problems present some of the most difficult challenges in the field of computational mechanics. In the case of nonlinear hyperelastic membrane structures undergoing large deformations and contact, the problem is even more acute due to the geometric and material nonlinearities. Such structures are found in various applications such as soft machines, vibration damping/isolation (tires, airsprings etc.), and terrestrial and space structures (see Jenkins (2001)). Inflated membranes with interactions are also found in procedures like angioplasty and thermoforming. Therefore, understanding the mechanics of contact in various membrane geometries is of fundamental importance and provides a motivation for the present study.

Feng and Yang (1973) investigated the deformation of a pressurized spherical balloon kept between two large frictionless rigid plates. Indentation problem of membranes were studied by Bhatia and Nachbar (1968), Yang and Hsu (1971) and Selvadurai and Yu (2006) for various geometries and indentors. Finite deformation of membranes with frictionless contact conditions was studied by Feng and Yang (1973), Feng et al. (1974), Feng and Haung (1975), Sohail and Nadler (2011) and Pearce et al. (2011). Feng (1987) has studied the indentation of a plane membrane with a parabolic indentor. Szyszkowski and Glockner (1984, 1987), Dacko and Glockner (1988) and Nadler (2010) have studied the finite deformation of spherical membranes under various loading conditions and observed the wrinkling phenomenon in these membranes. Khayat and Derdouri (1993) have studied the confined axisymmetric inflation of a hyperelastic isotropic and homogeneous cylindrical membrane, with fixed ends. The Mooney–Rivlin constitutive model has been considered in the analysis with non-uniform radius and thickness distribution of the cylinder in the undeformed configuration. The problem has been formulated to account for single and multiple contacts. Konyukhov and Schweizerhof (2004, 2005) have developed a general mathematical framework for solving large deformation frictionless contact problems using closest point projection method. Experimental and computational studies on the indentation mechanics of flat membranes with axisymmetric and asymmetric deflections have been carried out recently by Selvadurai (2006) and Selvadurai and Shi (2012). Long et al. (2010) have considered the adhesive contact problem of an inflated hyperelastic membrane with a flat rigid plate. They have solved the contact problem with slip, no-slip and adhesive contact conditions. Recently, Kumar and DasGupta (2013) have addressed the problem of deformation of an inflated spherical membrane between two rigid flat plates with frictionless, no-slip and finite frictional contact conditions. They have also determined the wrinkling conditions for the membrane analytically.

* Corresponding author. Tel.: +91 9734427136.
E-mail addresses: ganesh@cts.iitkgp.ernet.in (G. Tamadapu), anir@mech.iitkgp.ernet.in (A. DasGupta).

0020-7683/$ - see front matter © 2013 Elsevier Ltd. All rights reserved.
http://dx.doi.org/10.1016/j.ijsolstr.2013.10.016

The wrinkling instability of membranes under anisotropic stretching has been addressed previously in different contexts by a number of authors (see, e.g., Steigmann (1990), Haseganu and Steigmann (1994), Li and Steigmann (1995) and Roxburgh (1995)). The issue of wrinkling instability in contact problems has been considered in the work of Nadler (2010). In the case of toroidal membranes, depending on the geometry parameter, even unconstrained inflation can lead to wrinkling, as observed by Tamadapu and DasGupta (2013). The occurrence of the wrinkled state in a membrane may lead to a loss of stiffness/integrity of the membrane structure. Hence, detection of the impending wrinkling state during inflation/deformation is an important part of the study in membrane contact problems.

In most of the existing literature, contact problems have been studied for flat circular, spherical and cylindrical shaped membranes. While the inflation of toroidal membranes has been studied to some extent (see, e.g., Kydoniefs and Spencer (1965), Hill (1980) and Tamadapu and DasGupta (2013)), the contact problem has not been explored. The complexity of the inflation-with-contact problem stems from the material and geometric nonlinearities associated with the inflation problem, and the varying curvature of the toroidal geometry. On the other hand, the toroidal geometry has application in inflatable tire tubes, antenna structures and arches. In some of these applications, interaction at the internal/external equator is expected. We intended to address the contact problem during inflation of a toroidal membrane over a frictionless cylindrical rim. Recently Tamadapu and DasGupta (2013) have presented the finite inflation analysis of toroidal membrane. They have reported that for high values of C_2/C_1 (where C_1 and C_2 are the Mooney–Rivlin material constants) the inner equator of the torus shrinks. Hence, toroidal membranes of such materials, when inflated, will form contact in the presence of an inner rim.

In this paper, we start with a general variational formulation of axisymmetric inflation of a toroidal membrane over a compliant and rigid inner cylindrical rim at the inner equator. The compliant cylinder is modeled as a linear distributed stiffness. The membrane–cylinder contact is assumed to be frictionless. The plane containing the inner and the outer equators of the torus is assumed to be a plane of symmetry. A general axisymmetric displacement field has been considered in the laboratory frame and the strain energy is considered in the Mooney–Rivlin form. For the case of contact with a compliant cylinder, the total potential energy comprising the strain energy, pressure work and the cylinder–membrane interaction energy is minimized to obtain the equilibrium equations. In the case of a rigid cylindrical contact, the equations of equilibrium are obtained separately for the contact and the non-contact regions. The equilibrium equations are solved using a shooting method with two (for compliant cylinder) and three (for rigid cylinder) dimensional search space. We have also studied the effect of the various parameters on the state of stretch and stress, and on the geometry of the inflated membrane. The occurrence of impending wrinkling state has been visualized on the principal stretch parameter plane. Some interesting observations have been highlighted.

The paper is organized as follows. In Section 2, we discuss the geometry of deformation of the toroidal membrane over various contacting surfaces. The variational formulation of the inflation problem has been presented in Section 3. The solution procedure is discussed in Section 4, and the numerical results are presented in Section 5. The paper is concluded with Section 6.

2. Kinematics of deformation

Consider a homogeneous, isotropic, hyperelastic toroidal membrane of circular cross-section with undeformed ring radius R, sectional radius r and thickness h. A circular cylinder of undeformed radius equal to the inner equator radius of the torus is surrounded by the toroidal membrane as shown Fig. 1. The contact between the torus and the cylinder is assumed to be frictionless. We assume that the thickness of the membrane is small compared to the characteristic dimensions of the torus. Let θ (meridional) and ϕ (circumferential) be the convected coordinates on the surface of the torus as shown in the figure. Let ξ be the coordinate along the local normal with $\xi = 0$ representing the mid-surface of the torus. The infinitesimal distance ds between two neighboring points on the torus can be represented as

$$\mathrm{d}s^2 = r^2\mathrm{d}\theta^2 + (R + r\cos\theta)^2\mathrm{d}\phi^2 + \mathrm{d}\xi^2.$$

Therefore, the components of the undeformed metric tensor are given by

$$[g_{ij}] = \begin{pmatrix} r^2 & 0 & 0 \\ 0 & (R + r\cos\theta)^2 & 0 \\ 0 & 0 & 1 \end{pmatrix}, \quad [g^{ij}] = [g_{ij}]^{-1}.$$

We assume that Y^3 and $Y^1 - Y^2$ remain, respectively, the axis and the plane of symmetry, and the cylinder is constrained during the inflation of the membrane. Let the material point $\mathcal{B}$ (deflected from $\mathcal{B}_0$) on the mid-surface of the membrane be represented by (ρ, η) in the laboratory frame, and $\mathcal{B}_c$ be the material point at the junction of the non-contacting and the contacting region of the membrane as shown in Fig. 1. Let Γ be the angular location (measured as shown in Fig. 1) of a material point in the undeformed state of the membrane that moves to $\mathcal{B}_c$ in the inflated configuration. The position vector of a point on the deformed torus is given by

$$p^i = y^i + \xi\,\lambda_3\,n^i. \tag{1}$$

Here,

$$y^1 = \rho(\theta)\cos\phi, \quad y^2 = \rho(\theta)\sin\phi, \quad y^3 = \eta(\theta) \tag{2}$$

and n^i is the unit outward normal vector to the deformed membrane surface given by

$$n^i = \frac{1}{2}\delta^{il}\varepsilon^{\alpha\beta}\varepsilon_{ljk}y^j_{,\alpha}y^k_{,\beta}, \text{ (summation convention)} \tag{3}$$

where $\varepsilon^{\alpha\beta} = e^{\alpha\beta}/\sqrt{G}$ and $\varepsilon_{ijk} = e_{ijk}$ are, respectively, the completely antisymmetric contravariant (two dimensional) and covariant (three dimensional) Levi-Civita tensors. Here,

$$y^i_{,\alpha} = \frac{\partial y^i}{\partial x^\alpha}, \quad (x^1, x^2) = (\theta, \phi) \tag{4}$$

are the two orthogonal vectors on the tangent plane of the deformed membrane surface. The corresponding components of the deformed metric tensor are then given by

$$[G_{ij}] = \begin{pmatrix} \rho'^2 + \eta'^2 & 0 & 0 \\ 0 & \rho^2 & 0 \\ 0 & 0 & \lambda_3^2 \end{pmatrix}, \tag{5}$$

where $(\cdot)' = \mathrm{d}(\cdot)/\mathrm{d}\theta$. The in-plane principal stretches of the membrane are given by

$$\lambda_1 = \frac{\sqrt{\rho'^2 + \eta'^2}}{r}, \tag{6}$$

$$\lambda_2 = \frac{\rho}{R + r\cos\theta}. \tag{7}$$

The third principal stretch in the thickness direction is given by

$$\lambda_3 = H/h, \tag{8}$$

where H is the deformed thickness.

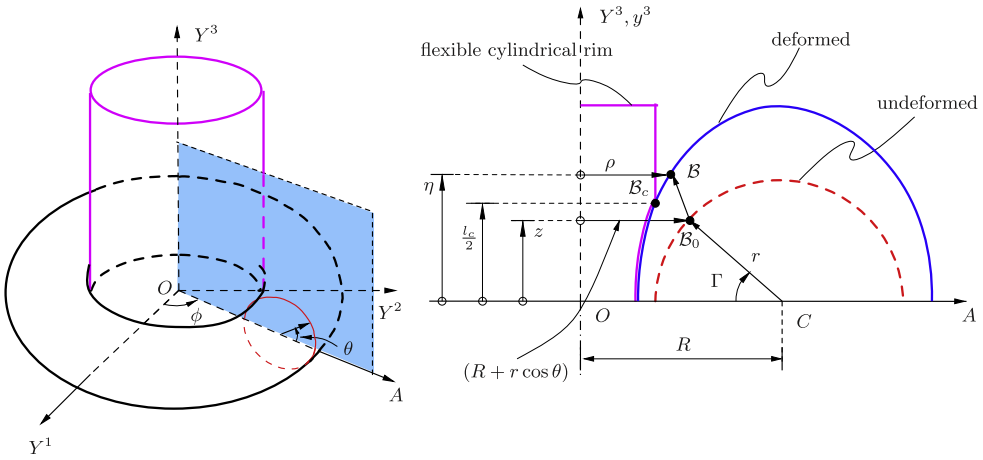

Fig. 1. A toroidal membrane in undeformed and deformed configurations over a compliant circular cylinder (modeled as a linear distributed stiffness).

3. Variational formulation

3.1. Material strain energy

For an isotropic incompressible and hyperelastic material, the Mooney–Rivlin strain energy density function (per unit undeformed volume) may be expressed as

$$\widehat{V} = C_1(I_1 - 3) + C_2(I_2 - 3) \tag{9}$$

where C_1 and C_2 are the usual material parameters, and $I_1 = [g^{ij}][G_{ij}]$ and $I_2 = [g_{ij}][G^{ij}]$ are the strain invariants of the right Cauchy–Green deformation tensor $[g^{ik}][G_{kj}]$. Incompressibility of the membrane material implies $\lambda_3^2 = g/G$, where g and G are the surface metric determinants in the undeformed and deformed configurations.

3.2. Pressure work

The work done by the inflating gas with (gage) pressure P is given as

$$W = \int_0^{2\pi}\int_0^{2\pi} \frac{1}{2}P\rho^2\eta'\mathrm{d}\theta\mathrm{d}\phi. \tag{10}$$

3.3. Compliant cylinder–membrane interaction energy

The work done by the compliant cylinder on the torus during inflation is given by

$$W_k = -\int_0^{2\pi}\int_0^{2\pi} \frac{1}{2}k\mathcal{H}(R - r - \rho)(\rho - R + r)^2\sqrt{G}\mathrm{d}\theta\mathrm{d}\phi \tag{11}$$

where k is the distributed stiffness of the cylinder and $\mathcal{H}(\cdot)$ is the Heaviside step function.

3.4. Equilibrium equations

The equations of equilibrium and boundary conditions of a toroidal membrane inflating over a compliant and a rigid cylinder are now presented below.

3.4.1. Constrained inflation over a compliant cylinder

In this case, from axisymmetry, the total potential energy for the system can be expressed as

$$\Pi = 2\pi h\int_0^{2\pi}\left(-\widehat{V} - \frac{1}{2h}kJ\mathcal{H}(R - r - \rho)(\rho - R + r)^2 + \frac{1}{2h\sqrt{g}}P\rho^2\eta'\right)\sqrt{g}\mathrm{d}\theta \tag{12}$$

where $J = \sqrt{G/g}$. By the principle of minimum potential energy, the equations of equilibrium are obtained as follows

$$\begin{aligned}
&\frac{\mathrm{d}}{\mathrm{d}\theta}\left(\frac{\rho'}{r}(1 + C_2\lambda_2^2)\left(1 - \frac{1}{\lambda_1^4\lambda_2^2}\right)(1 + r\cos\theta)\right)\\
&\quad - r\lambda_2(1 + C_2\lambda_1^2)\left(1 - \frac{1}{\lambda_1^2\lambda_2^4}\right) + \frac{1}{2}P\rho\eta'\\
&\quad - \frac{1}{2}k\mathcal{H}(1 - r - \rho)\left(\frac{\rho'\eta'}{\sqrt{\rho'^2 + \eta'^2}}(\rho - 1 + r)(3\rho - 1 + r)\right.\\
&\quad \left. + \frac{(\rho - 1 + r)^2\rho\rho'\eta'^2}{(\rho'^2 + \eta'^2)^{3/2}}\frac{\mathrm{d}}{\mathrm{d}\theta}\left(\frac{\rho'}{\eta'}\right)\right) = 0,
\end{aligned} \tag{13}$$

$$\begin{aligned}
&\frac{\eta'}{r}(1 + C_2\lambda_2^2)\left(1 - \frac{1}{\lambda_1^4\lambda_2^2}\right)(1 + r\cos\theta)\\
&\quad - \frac{1}{4}P\rho^2 + \frac{1}{2}k\mathcal{H}(1 - r - \rho)(\rho - 1 + r)\frac{\rho\eta'}{\sqrt{\rho'^2 + \eta'^2}} = L,
\end{aligned} \tag{14}$$

where L is the integration constant. The boundary conditions for the membrane can be written as follows

$$\rho'(0) = \rho'(\pi) = 0 \quad \eta(0) = \eta(\pi) = 0. \tag{15}$$

The condition at the contact junction can be obtained from the term in the variational equation as given by

$$\int_0^{2\pi} kJ\,\delta(R - r - \rho)(\rho - R + r)^2\,\delta\rho\sqrt{g}\mathrm{d}\theta = 0 \tag{16}$$

where $\delta(\cdot)$ represents the Dirac delta function. Using the properties of the Dirac delta function in (16) gives the condition at the contact junction as

$$\rho(\pi - \Gamma) = R - r.$$

3.4.2. Constrained inflation over a rigid cylinder

The total potential energy of the system in this case is given by

$$\begin{aligned}
\Pi &= 2\pi h\int_0^{2\pi}\left(-\widehat{V} + \frac{1}{2h\sqrt{g}}P\rho^2\eta'\right)\sqrt{g}\,\mathrm{d}\theta\\
&= 2\pi h\left(\int_0^{\pi-\Gamma}\left(-\widehat{V} + \frac{1}{2h\sqrt{g}}P\rho^2\eta'\right)\sqrt{g}\,\mathrm{d}\theta\right.\\
&\quad \left. + \int_{\pi-\Gamma}^{\pi}\left(-\widehat{V}\Big|_{\substack{\bar{\rho}=(R-r)\\ \bar{\rho}'=0}} + \frac{1}{2h\sqrt{g}}P(R - r)^2\bar{\eta}'\right)\sqrt{g}\,\mathrm{d}\theta\right)
\end{aligned} \tag{17}$$

where $(\bar{\cdot})$ corresponds to the field variables in the contact region. By the principle of minimum potential energy, the equations of equilibrium, boundary conditions and junction conditions for the membrane are obtained separately for the non-contact and the contact regions and are given below.

Non-contacting region: The equations of equilibrium in the non-contact region $(0 \leqslant \theta \leqslant \pi - \Gamma)$ are given by

$$\frac{\mathrm{d}}{\mathrm{d}\theta}\left(\frac{\rho'}{r}(1+C_2\lambda_2^2)\left(1-\frac{1}{\lambda_1^4\lambda_2^2}\right)(1+r\cos\theta)\right) - r\lambda_2(1+C_2\lambda_1^2)\left(1-\frac{1}{\lambda_1^2\lambda_2^4}\right)+\frac{1}{2}P\rho\eta' = 0, \tag{18}$$

$$\frac{\eta'}{r}(1+C_2\lambda_2^2)\left(1-\frac{1}{\lambda_1^4\lambda_2^2}\right)(1+r\cos\theta)-\frac{1}{4}P\rho^2 = I, \tag{19}$$

where I is the integration constant. The boundary conditions of the membrane in the non-contact region may be written as

$$\rho'(0)=\rho'(\pi-\Gamma)=0, \quad \eta(0)=0, \quad \rho(\pi-\Gamma)=1-r. \tag{20}$$

Contacting region: The equation of equilibrium in the contact region is given by

$$\frac{\bar{\eta}'}{r}\left(1+C_2\frac{(1-r)^2}{(1+r\cos\theta)^2}\right) \times\left(1-\frac{r^4(1+r\cos\theta)^2}{\bar{\eta}'^4(1-r)^2}\right)(1+r\cos\theta)-\frac{1}{4}P(1-r)^2 = I. \tag{21}$$

The boundary condition for the membrane in the contact region is $\bar{\eta}(\pi)=0$. The junction condition at the contact point can be written as

$$\bar{\lambda}_1|_{\theta=\pi-\Gamma} = \lambda_1|_{\theta=\pi-\Gamma}.$$

For the Mooney–Rivlin strain energy density function, the non-dimensional Cauchy stress resultants T_1 (meridional) and T_2 (circumferential) are given by

$$T_1 = \lambda_3\lambda_1\frac{\partial\widehat{V}}{\partial\lambda_1} = 2\left(\frac{\lambda_1}{\lambda_2}-\frac{1}{\lambda_1^3\lambda_2^3}\right)(1+C_2\lambda_2^2) \tag{22}$$

$$T_2 = \lambda_3\lambda_2\frac{\partial\widehat{V}}{\partial\lambda_2} = 2\left(\frac{\lambda_2}{\lambda_1}-\frac{1}{\lambda_1^3\lambda_2^3}\right)(1+C_2\lambda_1^2). \tag{23}$$

In the rest of the paper, we use the non-dimensional quantities

$$(r,\rho,\eta)\to\frac{(r,\rho,\eta)}{R}, \quad C_2\to\frac{C_2}{C_1}, \quad P\to\frac{PR}{C_1h}, \quad (T_1,T_2)\to\frac{(T_1,T_2)}{C_1h}, \quad k\to\frac{kR^2}{C_1h}$$

and the scaling $C_1=1, h=1$ and $R=1$. Thus, we finally have four non-dimensional parameters in the problem namely, the geometric parameter r, the material parameter C_2, the stiffness parameter k (for the compliant cylinder only), and the inflation pressure P.

4. Solution procedure

4.1. Compliant cylinder in contact

The two point boundary value problem of the membrane (13)–(15) is converted to an initial value problem with two unknown initial conditions $\rho(0)$ and $\eta'(0)$ at a given pressure P. The additional constraints on the initial value problem are the other two boundary conditions $\rho(\pi)=0$ and $\eta(\pi)=0$. Here, $\rho(0)$ is the net horizontal displacement of a point on the outer equator of the membrane, which can be taken to be greater than $(1+r)$ and must be a single valued function of pressure. Therefore, assuming the inflation pressure as an unknown parameter for an assumed value of $\rho(0)$, an optimization function is constructed for the shooting method with the optimization parameters P and $\eta'(0)$ as

$$S_c(\eta'(0),P) = \left[\rho'(\pi;\eta'(0),P)^2+\eta(\pi;\eta'(0),P)^2\right]^{1/2}. \tag{24}$$

We start with a small value of $\rho(0)(>(1+r))$ and with an initial guess pair $(\eta_i'(0),P_i)$. The shooting process is implemented to obtain an accurate final pair $(\eta_f'(0),P_f)$ through Nelder–Meads search technique such that $S_c(\eta_f'(0),P_f)<e_{max}$, where e_{max} is an arbitrarily small positive constant. The value of $\rho(0)$ is increased further in small steps and the shooting process is repeated with the solution of the previous iteration as the initial guess. The above process is continued until initial conditions $\rho(0)$ and $\eta'(0)$ are obtained for different values of the inflation pressure. For improving the computational efficiency, at the start of each iteration for an incremental increase in the displacement of the outer equator, a new initial guess pair is obtained using a cubic extrapolation in the two dimensional space of the pair. Later, these initial conditions are used to find the principal stretches and the equilibrium configurations of the membrane for different inflation pressures.

4.2. Rigid cylinder in contact

In the contact region, the two point boundary value problem of the membrane (18)–(20) is converted to an initial value problem with three unknowns $\rho(0),\eta'(0)$ and P at an assumed contact angle Γ. The additional constraints on the initial value problem are the other two boundary conditions $\rho(\pi-\Gamma)=1-r, \rho'(\pi-\Gamma)=0$ and the contact condition $\bar{\lambda}_1|_{\theta=\pi-\Gamma}=\lambda_1|_{\theta=\pi-\Gamma}$. An optimization function is constructed for the shooting method with the optimization parameters $\rho(0),\eta'(0)$ and P as

$$S_r(\mathbf{X}) = \Big[\{\rho(\pi-\Gamma;\mathbf{X})-1+r\}^2+\{\rho'(\pi-\Gamma;\mathbf{X})\}^2 + \{\lambda_1(\pi-\Gamma;\mathbf{X})-\bar{\lambda}_1(\pi-\Gamma;\mathbf{X})\}^2\Big]^{1/2} \tag{25}$$

where $\mathbf{X}$ is the parameter vector given by $\mathbf{X}=(\rho(0),\eta'(0),P)^T$. We perform the following steps to solve the contact problem. We start with a small value of Γ with the initial guess triplet $\mathbf{X}_i$. Using the guess triplet, the value of the constant I is calculated from (19), and used to solve (21) to obtain the value of $\bar{\lambda}_1(\pi-\Gamma;\mathbf{X})$. Then, (18) and (19) are solved to find the value of the optimization function $S_r(\mathbf{X})$. The shooting process is implemented to obtain an accurate final vector $\mathbf{X}_f$ through Nelder–Meads search technique such that $S_r(\mathbf{X}_f)<e_{max}$. The value of Γ is increased further in small steps and the shooting process is repeated with the previous iteration triplet solution as the initial guess. The above process is continued until the solution vector $\mathbf{X}$ is obtained for different values of the contact angle. For improving the computational efficiency, at the start of each iteration for an incremental increase in the contact angle, a new initial guess triplet is obtained using a cubic extrapolation in the three dimensional space of triplets. The solution triplets obtained finally are used to calculate the principal stretches, Cauchy stress resultants and the equilibrium configurations of the membrane at the different contact angles considered.

5. Numerical results and discussions

We first present and discuss the variation of the principal stretches with pressurization of a toroidal membrane over a frictionless compliant and rigid cylindrical surfaces placed at the inner

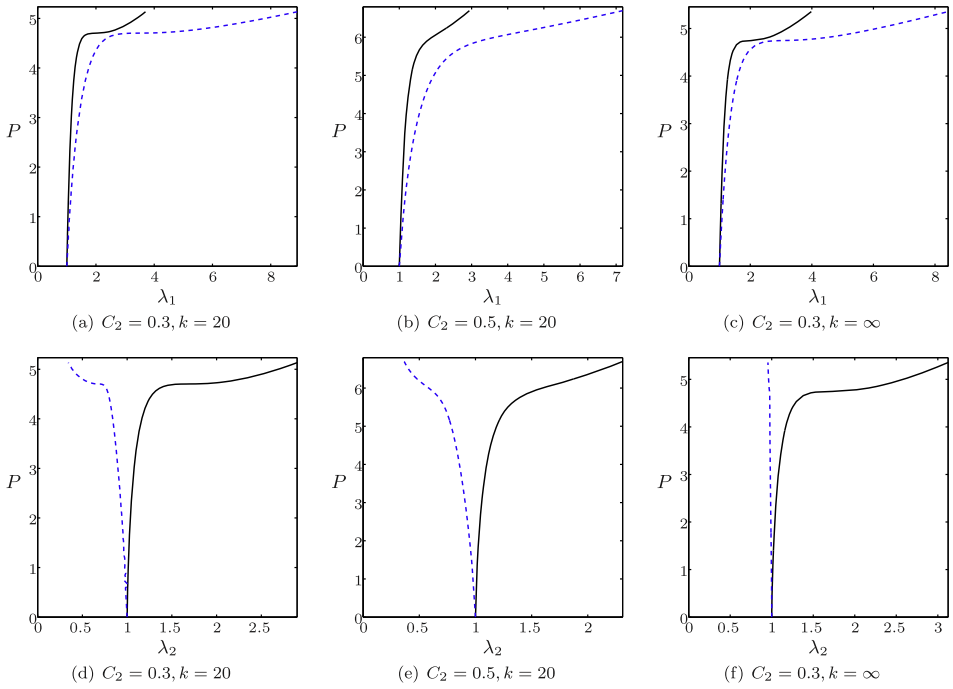

Fig. 2. Variation of the inflation pressure with meridional (λ_1) and circumferential (λ_2) stretches for the inflation of toroidal membrane over a compliant cylinder ((a), (b), (d) and (e)) at $\theta = 0$ (——), π (– – – –) and rigid cylinder ((c) and (f)) at $\theta = 0$ (——), $\pi - \Gamma$ (– – – –).

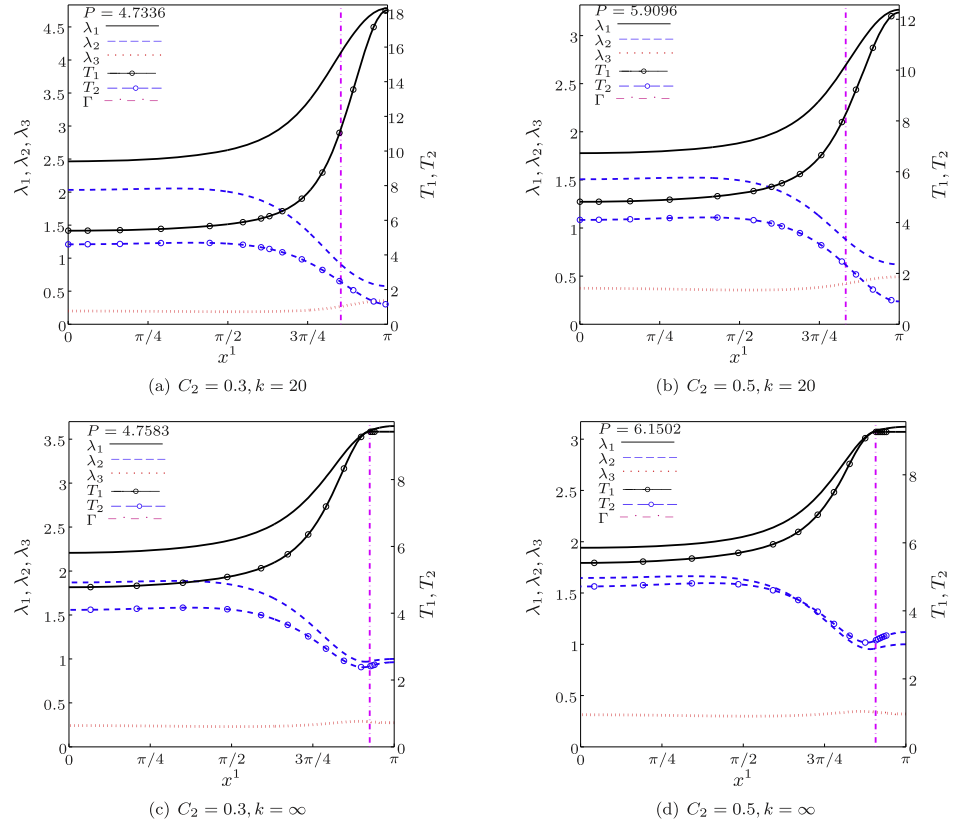

Fig. 3. The variation of the principal stretches and the Cauchy stress resultants of a toroidal membrane inflating over a compliant ((a) and (b)) and rigid ((c) and (d)) cylinder at a particular inflation pressure. The dot-dashed line indicates the contact junction in the undeformed configuration.

equator of the torus. For the finite inflation of a toroidal membrane, the movement of the inner equator towards the center of the torus during inflation can be attained for values of $C_2 > 0.214$ (Tamadapu and DasGupta, 2013). Therefore, to maintain the contact between the cylinder and the torus during inflation, high values of C_2 are considered in the analysis. The crossing of the

principal stretch solutions with zero Biot stress boundaries are discussed later for the identification of impending wrinkling condition in the membrane with the inflation pressure. The Cauchy stress resultants, contact length and normal stress acting on the compliant cylinder are calculated and discussed. In all our numerical computations, we have taken $r = 0.5$ (unless specified otherwise) and $e_{max} = 10^{-10}$.

5.1. Deformation of the membrane over a cylindrical rim with frictionless contact

The variation of the inflation pressure with the principal stretches of the toroidal membrane are shown in Fig. 2. For the case of a compliant cylindrical rim with $k = 20$, the variation of the inflation pressure with principal stretches for $C_2 = 0.3, 0.5$ are shown in Fig. 2(a), (b), (d) and (e) at $\theta = 0, \pi$. For the case of a rigid cylindrical rim, the variation of the inflation pressure with principal stretches for $C_2 = 0.3$ is shown in Fig. 2(c) and (f) at $\theta = 0, \pi - \Gamma$.

From Fig. 2(a) and (c), it is interesting to observe that increase in the stiffness of the cylinder from $k = 20$ to $k = \infty$ (rigid cylinder) has no affect on the critical/inflexion point pressure and the meridional stretch of the membrane. Further, comparing the results of Tamadapu and DasGupta (2013); (figure not reproduced here) with the results in Fig. 2, it is interesting to note that the inflexion point pressure does not change in the presence of the interaction with the rim. Thus, it is dependent on the material parameters and geometry. However, the circumferential stretch (in Fig. 2(d) and (f)) shows a marked variation due to the increasing strength of obstruction (due to the rim) with increasing stiffness of the rim. Due to the obstruction in material flow towards the center of the torus, maximum (minimum) meridional (circumferential) stretch is expected at the contact junction.

The variation of the principal stretches and the Cauchy stress resultants along the meridian of the toroidal membrane inflating on compliant and rigid cylindrical rims are shown in Fig. 3 for particular values of the inflation pressure. It is observed that the principal stretches and Cauchy stress resultants are all continuous with continuous gradients. This is because of the fact that the contact is frictionless. In case of frictional/adhesive contact, gradient discontinuities will arise (as observed by Kumar and DasGupta (2013) in a different context). In all the cases, we note that the maximum value of the meridional stretch (λ_1) (as well as the Cauchy stress T_1) occurs always at the inner equator of the toroidal membrane. However, as seen in Fig. 3(c) and (d) for the rigid cylinder, the circumferential stretch (λ_2) is less than unity in the contacting region, and surprisingly the minimum, close to the contact junction (in the non-contacting region at an angle $\Lambda\,(>\Gamma)$ measured in the clockwise direction from the inner equator). The circumferential Cauchy stress resultant also exhibits a similar trend. This is contrary to that in the case of the compliant cylinder (see Fig. 3(a) and (b)) for which the minimum Cauchy stress is observed at the inner equator. This feature has an important consequence in terms of wrinkling instability, as discussed in the following.

5.2. Impending wrinkling condition

To identify the point of impending wrinkling condition in the equilibrium solutions, following the analysis of Tamadapu and DasGupta (2013), the domain of the solutions is plotted on the

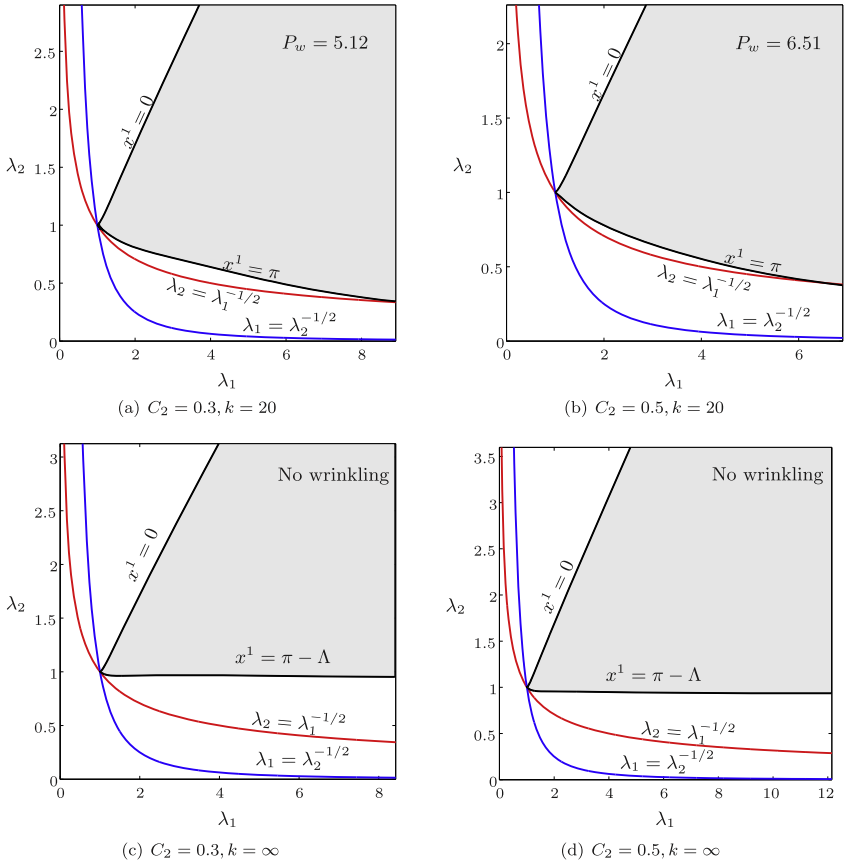

Fig. 4. Principal stretch values (shaded region) for all possible inflation pressure values on the $\lambda_1 - \lambda_2$ plane with the zero principal Biot stress boundaries $\lambda_2 = \lambda_1^{-1/2}$ and $\lambda_1 = \lambda_2^{-1/2}$ for the toroidal membrane inflation over a compliant ((a) and (b) with boundaries at $x^1 = 0, \pi$) and rigid ((c) and (d) with boundaries $x^1 = 0, \pi - \Lambda$) cylinder.

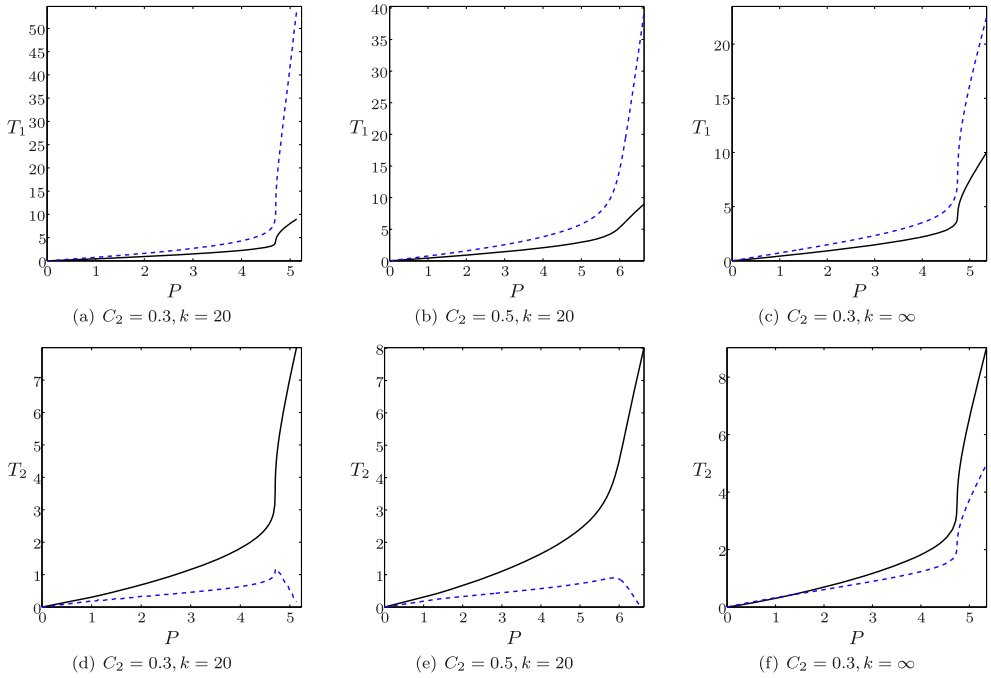

(a) $C_2 = 0.3, k = 20$ (b) $C_2 = 0.5, k = 20$ (c) $C_2 = 0.3, k = \infty$

(d) $C_2 = 0.3, k = 20$ (e) $C_2 = 0.5, k = 20$ (f) $C_2 = 0.3, k = \infty$

Fig. 5. Variation of the Cauchy stress resultants with the inflation pressure of a toroidal membrane inflating over a compliant cylinder (for (a), (b), (d) and (e) at $\theta = 0$ (———), π (– – – –)) and rigid cylinder (for (c) and (f) at $\theta = 0$(———), $\pi - \Gamma$ (– – – –)).

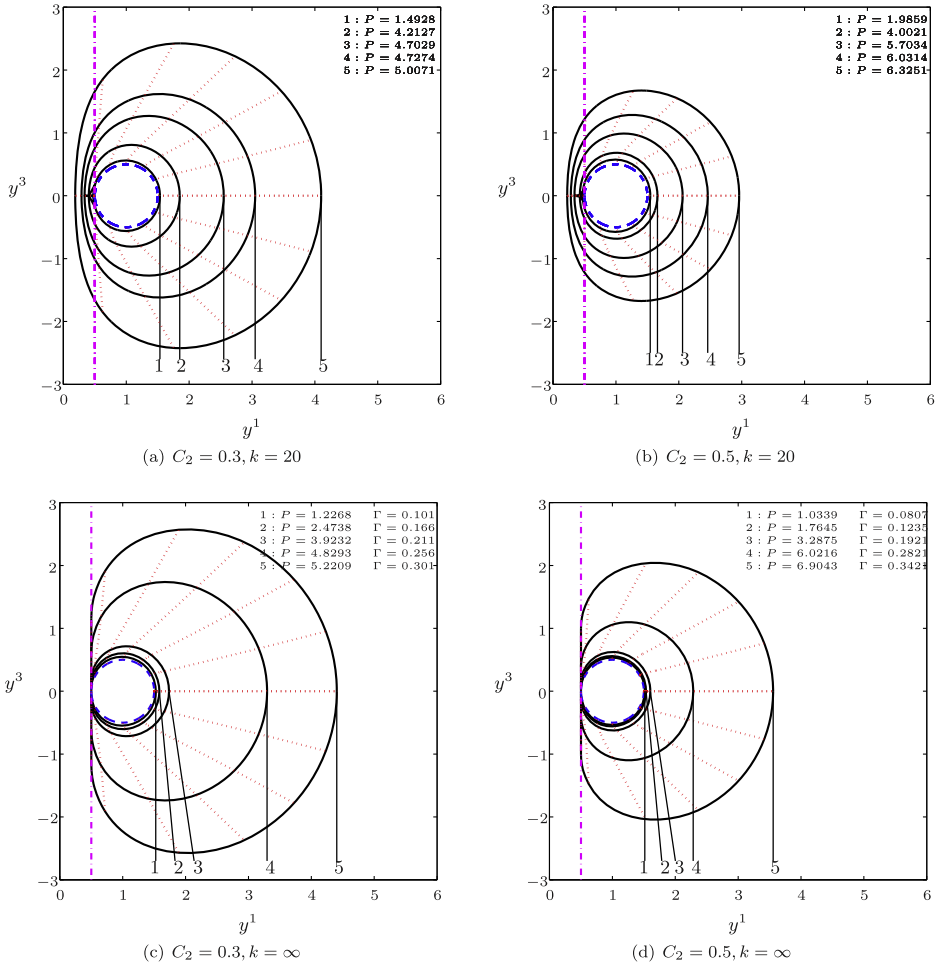

(a) $C_2 = 0.3, k = 20$ (b) $C_2 = 0.5, k = 20$

(c) $C_2 = 0.3, k = \infty$ (d) $C_2 = 0.5, k = \infty$

Fig. 6. Deformed cross-sections of a torus with $r = 0.5$ (dashed configuration) inflating over a compliant cylinder ((a), (b)) and a rigid cylinder ((c), (d)) for certain inflation pressures. The dotted lines represent the motion of the material points during inflation, and the dot-dashed line represents the boundary of the cylindrical rim in the undeformed configuration.

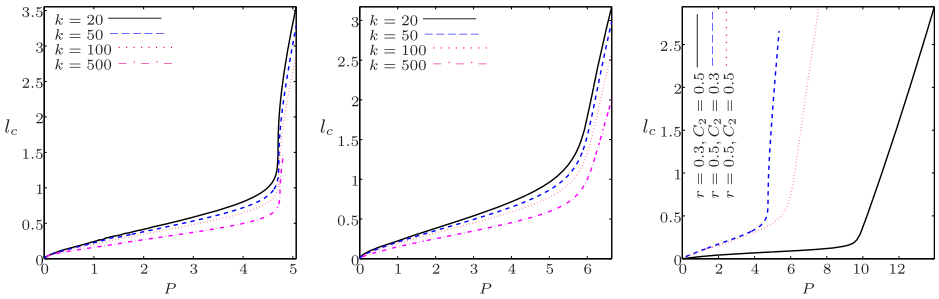

(a) $C_2 = 0.3$ (b) $C_2 = 0.5$ (c)

Fig. 7. Variation of the contact length with the inflation pressure for compliant ((a) and (b)) and rigid cylinder (c) cases.

principal stretch parameter plane along with the region of stability for the pressure range considered. The crossing of the solution domain boundary with the stability boundary indicates the impending wrinkling state in the membrane and puts a limit on the solution for no wrinkling. These results are presented in Fig. 4 for the inflation of the toroidal membrane (with material parameter values $C_2 = 0.3, 0.5$) over a compliant ($k = 20$) and rigid cylindrical rims. The corresponding value of the pressure at which impending wrinkling condition occurs is also indicated in the plots. The shaded region in these figures indicate the domain of the two principal stretches of the membrane for all possible values of the inflation pressure. The boundary of the shaded region indicates the minimum meridional and circumferential principal stretches at a given pressure obtained from $d\lambda_i/dx^1 = 0$, as indicated in the figures. It is found that the minimum circumferential principal stretch occurs at $x^1 = \pi$ and $x^1 = \pi - \Lambda$ for the compliant and rigid cylindrical rims, respectively. On the other hand, the minimum meridional stretch occurs at $x^1 = 0$ for all the cases. The stability boundaries (zero principal Biot stress boundaries $\partial\widehat{V}/\partial\lambda_i$=0) on the stretch plane are represented by the two curves $\lambda_1 = \lambda_2^{-1/2}$ and $\lambda_2 = \lambda_1^{-1/2}$ (see Klisch (2007) and Ogden (2003)). Tamadapu and DasGupta (2013) have observed the impending wrinkling phenomenon during free inflation of the toroidal membrane for higher values of C_2 at $r = 0.5$. Here, for the case of the compliant cylindrical contact, as shown in Fig. 4(a) and (b), the crossing of the solution boundary with the stability boundary is observed in the pressure range considered. Surprisingly, no impending wrinkling condition is observed for the case of the rigid cylindrical contact, as shown in Fig. 4(c) and (d) even with large meridional stretch at the inner equator. It was observed in Tamadapu and DasGupta (2013) that wrinkling occurs due to the extension of the meridional fibers and contraction of the circumferential fibers. The reason for this was traced to the negative curvature around the inner equator. Hence, if the inner equator is restricted against

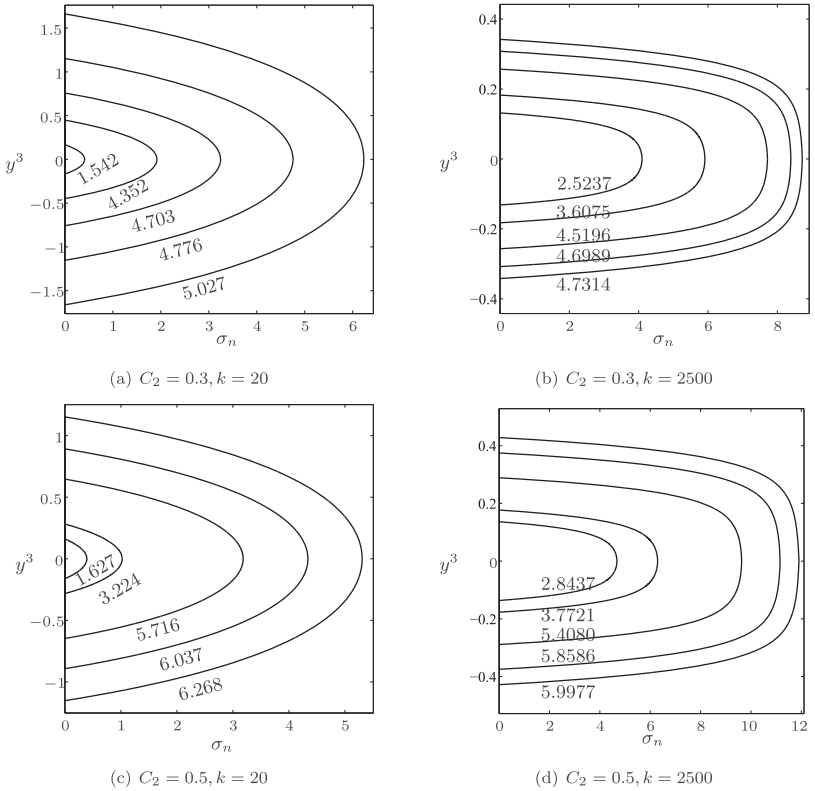

(a) $C_2 = 0.3, k = 20$ (b) $C_2 = 0.3, k = 2500$

(c) $C_2 = 0.5, k = 20$ (d) $C_2 = 0.5, k = 2500$

Fig. 8. The contact stress acting on the compliant cylinder in the contacting region at different inflation pressures of the toroidal membrane with material parameter values $C_2 = 0.3, 0.5$ and stiffness values of the cylinder $k = 20, 2500$.

contraction, the circumferential Cauchy stress is lower bounded (as observed in Fig. 3(c) and (d). This eliminates the possibility of occurrence of compressive stress in the membrane, and thus, wrinkling is prevented in the case of a rigid rim. It is interesting to note that, with the increase in the stiffness of the cylinder and the material parameter of the torus, the membrane can withstand higher inflation pressure before the impending wrinkling condition sets in.

5.3. Cauchy stress resultants

The variation of the Cauchy stress resultants with the inflation pressure are shown in Fig. 5 for both compliant ($k = 20$) and rigid cylindrical contact conditions at $x^1 = 0, \pi$ and $x^1 = 0, \pi - \Gamma$, respectively. It is observed from Fig. 3(a) and (b) that the Cauchy stress resultant T_1 (T_2) along the meridian is maximum (minimum) at the inner equator for the case of a flexible cylindrical rim. For the case of the rigid cylindrical rim, the Cauchy stress resultant T_1 (T_2) along the meridian is maximum (minimum) at the inner equator (near to the contact junction). From Fig. 5(a), (b), (d) and (e), it is noted that the toroidal membrane can withstand larger inflation pressures with smaller values of the stress resultants before which the circumferential stress resultant becomes zero (impending wrinkling condition). From Fig. 5(a), (b), (c) and (f), it is interesting to note that the value of the Cauchy stress resultant T_1 (T_2) decreases (increases) at the inner equator with the increase in the stiffness of the cylinder from $k = 20$ to $k \to \infty$.

5.4. Variation of geometric shape

The change in the cross-sectional shape of the toroidal membrane during inflation is shown in Fig. 6 for compliant and rigid cylindrical surfaces. It may be noted that, in the case of the compliant cylindrical rim, the cylinder surface in the contacting region conforms with the deformed membrane shape. Further, while the slope of the membrane for both cases (compliant and rigid rims) is continuous at all points, the deformed compliant rim has a slope discontinuity at the contact line. This is to be expected for a compliant surface modeled as a distributed stiffness.

The inflated shapes of the toroidal membrane with $r = 0.5$ over a compliant cylinder ($k = 20$) are shown in Fig. 6(a) and (b) for the material parameter values $C_2 = 0.3, 0.5$. The inflated shapes of the toroidal membrane over a rigid cylinder are shown in Fig. 6(c) and (d) for the material parameter values $C_2 = 0.3$ and 0.5, respectively. In all these figures, the path followed by the material point during the inflation process is indicated along with the location of the cylinder in the undeformed configuration. For the case of inflation over the rigid cylinder, the corresponding contact junction angles are also indicated. As expected, with the increase in the stiffness of the cylinder for a given material parameter the movement of the inner equator towards the center of the torus reduces. On the other hand, for a given stiffness of the cylinder and inflation pressure, the cross-section of the toroidal membrane at the equilibrium configuration is larger for lower values of C_2. The paths followed by the material points during the inflation is almost linear except at lower pressures.

The variation in the contact length (l_c) of the toroidal membrane over the rim with variation in the inflation pressure for different material parameters is presented for a compliant cylinder in Fig. 7(a) and (b), and for a rigid cylinder in Fig. 7(c). It is observed that the contact length decreases with the increase in the material parameter of the toroidal membrane and stiffness of the cylindrical rim for a given value of the inflation pressure. This is due to the increase in stiffness of the membrane resulting in lower inflation and contact length.

5.5. Contact stress on the cylinder

The variation of the normal contact stress $\sigma_n = k(1 - r - \rho)$ acting on the compliant cylindrical rim in the contacting region is shown in Fig. 8 at certain inflation pressure values. With the increase in the stiffness of the cylinder for a given material parameter, the normal stress acting on the cylinder increases as expected. It is observed that the stress distribution tends to be uniform at higher pressure with increasing stiffness of the rim.

6. Conclusions

The finite inflation of a hyperelastic homogeneous and isotropic toroidal membrane interacting with an inner cylindrical rim with frictionless contact conditions is considered in this paper. Both, compliant and rigid rims are considered in the analysis. The Mooney–Rivlin material model with large values of the material strain-hardening parameter is considered since it ensures the maintenance of the contact between the cylinder and the membrane upon inflation. The equilibrium equations obtained using the principle of minimum potential energy are solved numerically as a two-point boundary value problem by shooting method. We have studied the effect of the geometric and material parameters of the torus, and the stiffness of the cylindrical rim on the equilibrium deformation mechanics of the membrane. The solutions obtained are verified on the principal stretch parameter plane for the impending wrinkling condition. The main results are summarized as follows.

- The effects of the rim stiffness and contact conditions (free inflation/contact inflation) on the inflexion point pressure of the membrane are negligible. Therefore, it can be concluded that the inflexion point pressure is an intrinsic property of the structure which can only depend on the material and geometric parameters of the membrane.
- For the case of a membrane inflating over a rigid cylinder, the circumferential stretch is observed to be lower bounded, and attains a minimum value close to the contact junction.
- The meridional stretch at the inner equator for which the impending wrinkling condition occurs increases with the increase in the stiffness of the cylinder. For the case of a membrane inflating over a rigid cylinder, no impending wrinkling condition is observed.
- It is observed that with the increase in the material strain hardening parameter, the membrane can withstand higher inflation pressure at smaller meridional stretch value before the wrinkling instability sets in.
- The contact stress between the membrane and the cylindrical rim tends to be uniform with increasing pressure and stiffness of the rim.

The approach presented in this paper may be extended to study the inflation of toroidal membranes over rims of different geometries. Optimization of the rim geometry for a desirable contact stress distribution over the rim is a problem of practical interest. The study of inflation of a toroidal membrane over a surface with frictional contact will be a challenging problem.

The present study is restricted to the Mooney–Rivlin material model which has a certain range of validity depending on the stretch. However, it has been observed (see Beatty (1987)) that the Mooney–Rivlin model provides a satisfactory qualitative description of balloon inflation experiments. On the other hand, more sophisticated phenomenological and mechanistic models (such as Ogden, Arruda–Boyce and Gent etc.) have been proposed

in the past. Extending the study with such models would be an interesting exploration. However, restrictions may have to be put on the material parameters to ensure the maintenance of contact with the rim.

References

Beatty, M.F., 1987. Topics in finite elasticity: hyperelasticity of rubber, elastomers, and biological tissues-with examples. Appl. Mech. Rev. 40 (12), 1699–1734.

Bhatia, N., Nachbar, W., 1968. Finite indentation of an elastic membrane by a spherical indenter. Int. J. Non Linear Mech. 3 (3), 307–324.

Dacko, A., Glockner, P., 1988. Spherical inflatables under axisymmetric loads: another look. Int. J. Non Linear Mech., 0020-7462 23 (56), 393–407. http://dx.doi.org/10.1016/0020-7462(88)90037-6.

Feng, W., 1987. Indentation of a plane membrane with a rigid paraboloid. Int. J. Non Linear Mech. 22 (3), 261–265.

Feng, W.W., Haung, P., 1975. On the general contact problem of an inflated nonlinear plane membrane. Int. J. Solids Struct. 11, 437–448.

Feng, W.W., Yang, W.-H., 1973. On the contact problem of an inflated spherical nonlinear membrane. J. Appl. Mech. 40 (1), 209–214. http://dx.doi.org/10.1115/1.3422928.

Feng, W.W., Tielking, J.T., Huang, P., 1974. The inflation and contact constraint of a rectangular mooney membrane. J. Appl. Mech. 41, 979–984.

Haseganu, E.M., Steigmann, D.J., 1994. Analysis of partly wrinkled membranes by the method of dynamic relaxation. Comput. Mech. 14 (6), 596–614.

Hill, J.M., 1980. The finite inflation of a thick-walled elastic torus. Q. J. Mech. Appl. Math. 33 (4), 471–490.

Jenkins, C.H.M. (Ed.), 2001. Gossamer Spacecraft: Membrane and Inflatable Structures Technology for Space Applications, vol. 191. AIAA, Reston, Virginia.

Khayat, R.E., Derdouri, A., García-Rejón, A., 1993. Multiple contact and axisymmetric inflation of hyperelastic cylindrical membranes. Proc. IMechE, Part C: J. Mech. Eng. Sci. 207 (3), 175–183.

Klisch, S.M., 2007. A bimodular polyconvex anisotropic strain energy function for articular cartilage. J. Biomech. Eng. 129 (2), 250–258.

Konyukhov, A., Schweizerhof, K., 2004. Contact formulation via a velocity description allowing efficiency improvement in frictionless contact condition. Comput. Mech. 33, 165–173.

Konyukhov, A., Schweizerhof, K., 2005. Covariant description for frictionless contact problem. Comput. Mech. 35, 190–213.

Kumar, N., DasGupta, A., 2013. On the contact problem of an inflated spherical hyperelastic membrane. Int. J. Non Linear Mech. 57, 130–139 http://dx.doi.org/10.1016/j.ijnonlinmec.2013.06.015 .

Kydoniefs, A.D., Spencer, A.J.M., 1965. The finite inflation of an elastic torus. Int. J. Eng. Sci. 3 (2), 173–195.

Li, X., Steigmann, D.J., 1995. Point loads on a hemispherical elastic membrane. Int. J. Non Linear Mech. 30 (4), 569–581.

Long, R., Shull, K.R., Hui, C.-Y., 2010. Large deformation adhesive contact mechanics of circular membranes with a flat rigid substrate. J. Mech. Phys. Solids 58 (9), 1225–1242. http://dx.doi.org/10.1016/j.jmps.2010.06.007.

Nadler, B., 2010. On the contact of a spherical membrane enclosing a fluid with rigid parallel planes. Int. J. Non Linear Mech. 45 (3), 294–300.

Ogden, R.W., 2003. Nonlinear elasticity, anisotropy, material stability and residual stresses in soft tissue. In: Holzapfel, G., Ogden, R.W. (Eds.), Biomechanics of Soft Tissue in Cardiovascular Systems, CISM Courses and Lectures, vol. 441. Springer-Verlag, Vienna, pp. 65–108.

Pearce, S., King, J., Holdsworth, M., 2011. Axisymmetric indentation of curved elastic membranes by a convex rigid indenter. Int. J. Non Linear Mech., 0020-7462 46 (9), 1128–1138. http://dx.doi.org/10.1016/j.ijnonlinmec.2011.04.030.

Roxburgh, D.G., 1995. Inflation of nonlinearly deformed annular elastic membranes. Int. J. Solids Struct. 32 (14), 2041–2052.

Selvadurai, A.P.S., 2006. Deflections of a rubber membrane. J. Mech. Phys. Solids 54 (6), 1093–1119.

Selvadurai, A.P.S., Shi, M., 2012. Fluid pressure loading of a hyperelastic membrane. Int. J. Non Linear Mech. 47 (2), 228–239.

Selvadurai, A.P.S., Yu, Q., 2006. On the indentation of a polymeric membrane. Proc. R. Soc. Lond. A 462 (2065), 189–209. http://dx.doi.org/10.1098/rspa.2005.1572.

Sohail, T., Nadler, B., 2011. On the contact of an inflated spherical membrane-fluid structure with a rigid conical indenter. Acta Mech. 218, 225–235.

Steigmann, D.J., 1990. Tension-field theory. Proc. R. Soc. Lond. A 429 (1876), 141–173.

Szyszkowski, W., Glockner, P.G., 1984. Finite deformation and stability behaviour of spherical inflatables under axisymmetric concentrated loads. Int. J. Non Linear Mech. 19, 489–496.

Szyszkowski, W., Glockner, P.G., 1987. Spherical membranes subjected to concentrated loads. Eng. Struct., 0141-0296 9 (1), 45–52. http://dx.doi.org/10.1016/0141-0296(87)90040-X.

Tamadapu, G., DasGupta, A., 2013. Finite inflation analysis of a hyperelastic toroidal membrane of initially circular cross-section. Int. J. Non Linear Mech. 49, 31–39.

Yang, W.H., Hsu, K.H., 1971. Indentation of a circular membrane. J. Appl. Mech. 38, 227–230. http://dx.doi.org/10.1016/j.jmps.2010.06.007.